Journal of Electroceramics 6:1, 75–88, 2001

Cement-Based Electronics

D.D.L. CHUNG

Composite Materials Research Laboratory, State University of New York at Buffalo, Buffalo, NY 14260-4400, U.S.A.

Submitted April 6, 2000, Revised June 26, 2000; Accepted June 30, 2000

Abstract. Cement-based electronics in the form of electrical circuit elements (conductor and diode in the form of a pn-junction), sensors of strain and damage, thermistor and thermoelectric device are reviewed. They enable a concrete structure to provide electronic functions.

Keywords: cement, concrete, electronics, electric, diode, pn, sensor, thermoelectric.

Introduction

Cement, such as Portland cement, has long been used as a structural material. However, it can be used as an electronic material that provides electrical circuit elements (e.g., conductor, diode, etc.), sensors (e.g., strain sensor, damage sensor and thermistor) and thermoelectric devices. The use of a structural material for electronics enables a structure to provide electronic functions, thereby making the structure multifunctional and smart.

Due to the large volume of usage of structural materials such as cement, structural materials must be rather inexpensive. In contrast, conventional electronic materials such as semiconductors are relatively expensive, particularly when vacuum processing, single crystals and high purity are required. Therefore, the use of a structural material for electronics results in low-cost electronics.

A structural material must have good mechanical properties. In contrast, semiconductors tend to have poor mechanical properties. The use of a structural material for electronics results in electronics that are mechanically rugged.

This paper is a review of cement-based electronics—an emerging field which is scientifically rich and technologically relevant.

Background on Cement-matrix Composites

Cement-matrix composites include concrete (containing coarse and fine aggregates), mortar (containing fine aggregate but no coarse aggregate) and cement paste (containing no aggregate, whether coarse or fine). It also includes steel reinforced concrete, i.e., concrete containing steel reinforcing bars. Other fillers, called admixtures, can be added to the mix to improve the properties of the composite. Admixtures are discontinuous, so that they can be included in the mix. They can be particles, such as silica fume (a fine particulate) and latex (a polymer in the form of a dispersion). They can be short fibers, such as polymer, steel, glass or carbon fibers. They can be liquids such as methylcellulose aqueous solution, water reducing agent, defoamer, etc. Admixtures for rendering the composite electronic abilities, while maintaining or even improving the structural properties, are the focus of this article.

Cement-matrix composites for electronics include those containing short carbon fibers (for sensing strain, damage and temperature, for rendering p-type behavior and for electromagnetic radiation reflection), short steel fibers (for thermoelectricity and for rendering n-type behavior) and silica fume (for helping fiber dispersion). This section provides background on cement-matrix composites, with emphasis on carbon fiber cement-matrix composites.

Carbon fiber cement-matrix composites are structural materials that are gaining in importance quite rapidly due to the decrease in carbon fiber cost [1] and the increasing demand of superior structural and functional properties. These composites contain short carbon fibers, typically 5 mm in length, as the short fibers can be used as an admixture in concrete (whereas continuous fibers cannot be simply added to the concrete

mix) and short fibers are less expensive than continuous fibers. However, due to the weak bond between carbon fiber and the cement matrix, continuous fibers [2–4] are much more effective than short fibers in reinforcing concrete. Surface treatment of carbon fiber (e.g., by heating [5] or by using ozone [6,7], silane [8], SiO_2 particles [9] or hot NaOH solution [10]) is useful for improving the bond between fiber and matrix, thereby improving the properties of the composite. In the case of surface treatment by ozone or silane, the improved bond is due to the enhanced wettability by water. Admixtures such as latex [6,11] methylcellulose [6] and silica fume [12] also help the bond.

The effect of carbon fiber addition on the properties of concrete increases with fiber volume fraction [13], unless the fiber volume fraction is so high that the air void content becomes excessively high [14]. (The air void content increases with fiber content and air voids tend to have a negative effect on many properties, such as the compressive strength.) In addition, the workability of the mix decreases with fiber content [13]. Moreover, the cost increases with fiber content. Therefore, a rather low volume fraction of fibers is desirable. A fiber content as low as 0.2 vol. % is effective [15], although fiber contents exceeding 1 vol. % are more common [16–20]. The required fiber content increases with the particle size of the aggregate, as the flexural strength decreases with increasing particle size [21].

Effective use of the carbon fibers in concrete requires dispersion of the fibers in the mix. The dispersion is enhanced by using silica fume (a fine particulate) as an admixture [14,22–24]. A typical silica fume content is 15% by weight of cement [14]. The silica fume is typically used along with a small amount (0.4% by weight of cement) of methylcellulose for helping the dispersion of the fibers and the workability of the mix [14]. Latex (typically 15–20% by weight of cement) is much less effective than silica fume for helping the fiber dispersion, but it enhances the workability, flexural strength, flexural toughness, impact resistance, frost resistance and acid resistance [14,25,26]. The ease of dispersion increases with decreasing fiber length [24].

The improved structural properties rendered by carbon fiber addition pertain to the increased tensile and flexible strengths, the increased tensile ductility and flexural toughness, the enhanced impact resistance, the reduced drying shrinkage and the improved freeze-thaw durability [13–15,17–25,27–38]. The tensile and flexural strengths decrease with increasing specimen size, such that the size effect becomes larger as the fiber length increases [39]. The low drying shrinkage is valuable for large structures and for use in repair [40,41] and in joining bricks in a brick structure [42,43]. The functional properties rendered by carbon fiber addition pertain to the strain sensing ability [7,44–58] (for smart structures), the temperature sensing ability [59–63], the damage sensing ability [44,48,64–66], the thermoelectric behavior [61–63], the thermal insulation ability [67–69] (to save energy for buildings), the electrical conduction ability [70–79] (to facilitate cathodic protection of embedded steel and to provide electrical grounding or connection), and the radio wave reflection/adsorption ability [80–84] (for electromagnetic interference or EMI shielding, for lateral guidance in automatic highways, and for television image transmission).

In relation to the structural properties, carbon fibers compete with glass, polymer and steel fibers [18,27–29,32,36–38,85]. Carbon fibers (isotropic pitch based) [1,85] are advantageous in their superior ability to increase the tensile strength of concrete, even though the tensile strength, modulus and ductility of the isotropic pitch based carbon fibers are low compared to most other fibers. Carbon fibers are also advantageous in the relative chemical inertness [86]. PAN-based carbon fibers are also used [17,19,22,33], although they are more commonly used as continuous fibers than short fibers. Carbon-coated glass fibers [87,88] and submicron diameter carbon filaments [78–80] are even less commonly used, although the former is attractive for the low cost of glass fibers and the latter is attractive for its high radio wave reflectivity (which results from the skin effect). C-shaped carbon fibers are more effective for strengthening than round carbon fibers [89], but their relatively large diameter makes them less attractive. Carbon fibers can be used in concrete together with steel fibers, as the addition of short carbon fibers to steel fiber reinforced mortar increases the fracture toughness of the interfacial zone between steel fiber and the cement matrix [90]. Carbon fibers can also be used in concrete together with steel bars [91,92], or together with carbon fiber reinforced polymer rods [93].

In relation to most functional properties, carbon fibers are exceptional compared to the other fiber types. Carbon fibers are electrically conducting, in contrast to glass and polymer fibers, which are not conducting. Steel fibers are conducting, but their typical diameter

($\geq$60 μm) is much larger than the diameter of a typical carbon fiber (15 μm). The combination of electrical conductivity and small diameter makes carbon fibers superior to the other fiber types in the area of strain sensing and electrical conduction. However, carbon fibers are inferior to steel fibers for providing thermoelectric composites, due to the high electron concentration in steel and the low hole concentration in carbon.

Although carbon fibers are thermally conducting, addition of carbon fibers to concrete lowers the thermal conductivity [67], thus allowing applications related to thermal insulation. This effect of carbon fiber addition is due to the increase in air void content. The electrical conductivity of carbon fibers is higher than that of the cement matrix by about 8 orders of magnitude, whereas the thermal conductivity of carbon fibers is higher than that of the cement matrix by only one or two orders of magnitude. As a result, the electrical conductivity is increased upon carbon fiber addition in spite of the increase in air void content, but the thermal conductivity is decreased upon fiber addition.

The use of pressure after casting [94], and extrusion [95,96] can result in composites with superior microstructure and properties. Moreover, extrusion improves the shapability [96].

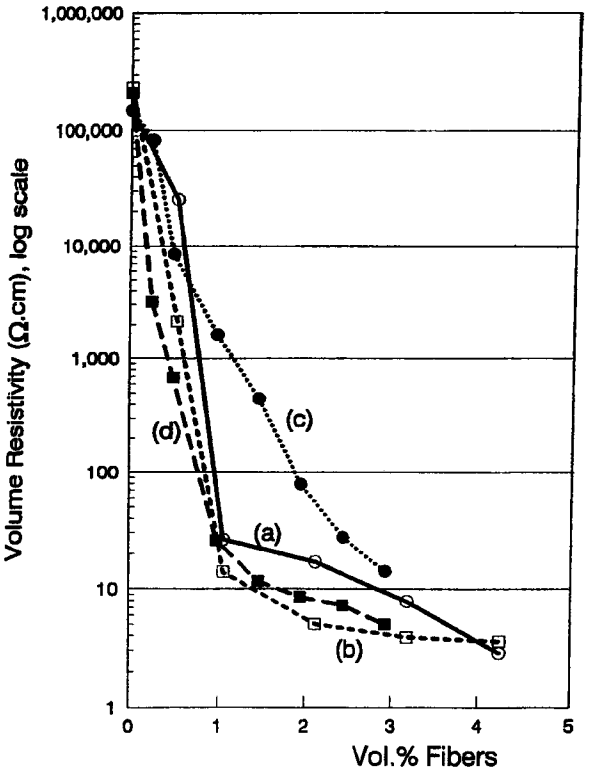

Fig. 1. Variation of the volume electrical resistivity with carbon fiber volume fraction. (a) Without sand, with methylcellulose, without silica fume; (b) Without sand, with methylcellulose, with silica fume; (c) With sand, with methyscellulose, without silica fume; (d) With sand, with methyscellulose, with silica fume.

Electrical Circuit Elements

Conductor

Short carbon fiber are particularly effective for enhancing the electrical conductivity of cement [75]. Fig. 1 [75] gives the volume electrical resistivity of composites at 7 days of curing. The resistivity decreases much with increasing fiber volume fraction, whether a second filler (silica fume or sand) is present or not. When sand is absent, the addition of silica fume decreases the resistivity at all carbon fiber volume fractions except the highest volume fraction of 4.24%; the decrease is most significant at the lowest fiber volume fraction of 0.53%. When sand is present, the addition of silica fume similarly decreases the resistivity, such that the decrease is most significant at fiber volume fractions below 1%. When silica fume is absent, the addition of sand decreases the resistivity only when the fiber volume fraction is below about 0.5%; at high fiber volume fractions, the addition of sand even increases the resistivity due to the porosity induced by the sand. Thus, the addition of a second filler (silica fume or sand) that is essentially non-conducting decreases the resistivity of the composite only at low volume fractions of the carbon fibers and the maximum fiber volume fraction for the resistivity to decrease is larger when the particle size of the filler is smaller. The resistivity decrease is attributed to the improved fiber dispersion due to the presence of the second filler. Consistent with the improved fiber dispersion is the increased flexural toughness and strength due to the presence of the second filler.

Diode

The pn-junction is the junction between a p-type conductor (a conductor with holes as the majority carrier) and an n-type conductor (a conductor with electrons as the majority carrier). The pn-junction is ideally recti-

fying, i.e., the current-voltage characteristic is such that the current is large when the applied voltage is positive on the p-side relative to the n-side and is small when the applied voltage is positive on the n-side relative to the p-side. The pn-junction is an electronic device that is central to electrical circuitry, due to its importance to diodes and transistors. Akin to the pn-junction is the n-n^+ junction, which is a junction between a weakly n-type conductor and a strongly n-type (i.e., n^+) conductor.

In the field of electrical engineering, a pn-junction is obtained by allowing a p-type semiconductor to contact an n-type semiconductor. These semiconductors are obtained by doping with appropriate impurities which serve as electrons donors (for n-type semiconductors) or electron acceptors (for p-type semiconductors).

Cement is inherently n-type, although it is only slightly n-type [63]. Upon addition of a sufficient amount of short carbon fibers to cement, a composite which is p-type is obtained [61–63]. Upon addition of short steel fibers to cement, a composite which is strongly n-type is obtained [97]. In other words, the cement matrix contributes to conduction by electrons; carbon fibers contribute to conduction by holes; steel fibers contribute to conduction by electrons.

Electric current rectification has been observed in a cement junction, as obtained by separate pouring of electrically dissimilar cement mixes side by side [98].

Fig. 2 shows the I-V characteristic for the junction involving carbon-fiber (1.0% by weight of cement) silica-fume cement paste (p-type, with absolute thermoelectric power -0.48 ± 0.11 μV/°C) and steel fiber (0.5% by weight of cement) cement paste (n-type, with absolute thermoelectric power 53.3 ± 4.8 μV/°C). This pn-junction is rectifying. The I-V characteristic is non-linear. The slope is steeper in the positive voltage regime than the negative voltage regime.

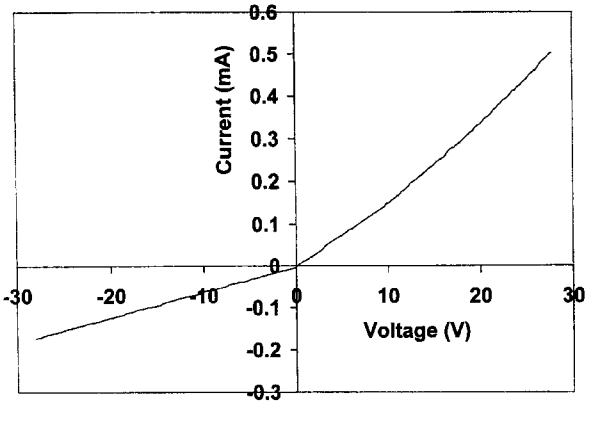

Fig. 2. I-V characteristic of a cement-based pn-junction.

The asymmetry in the I-V characteristic on the two sides of the origin for various junctions is in sharp contrast to the symmetry for a homogeneous piece of cement paste without a junction [59]. Hence, the asymmetry is attributed to the junction itself.

The junctions are rectifying; the magnitude of current is much larger when the voltage is positive than when the voltage is negative. The rectification is attributed to the asymmetric electron flow resulting from the junction. Due to the high concentration of electrons in the n-side, electrons predominantly flow by diffusion from the n-side to the p-side across the junction. This flow is enhanced by a positive voltage (i.e., forward bias), which lowers the contact potential at the junction. When the voltage is negative (i.e., reverse bias), the contact potential is high, causing the diffusion current to be low. However, electrons are swept from the p-side to the n-side under the electric field associated with the high contact potential at the junction, resulting in a drift current in the direction opposite to the diffusion current. The drift current is enhanced by a more negative voltage, but is low due to the low electron concentration in the p-side.

Sensors

Strain Sensor

The electrical resistance of strain sensing concrete (without embedded or attached sensors) changes reversibly with strain, such that the gage factor (fractional change in resistance per unit strain) is up to 700 under compression or tension [7,44–58]. The resistance (DC/AC) increases reversibly upon tension and decreases reversibly upon compression, due to fiber pull-out upon microcrack opening (<1 μm) and the consequent increase in fiber-matrix contact resistivity. The concrete contains as low as 0.2 vol.% short carbon fibers, which are preferably those that have been surface treated. The fibers do not need to touch one another in the composite. The treatment improves the wettability with water. The presence of a large aggregate decreases the gage factor, but the strain sensing ability remains sufficient for practical use. Strain sens-

ing concrete works even when data acquisition is wireless. The applications include structural vibration control and traffic monitoring.

Fig. 3(a) shows the fractional change in resistivity along the stress axis as well as the strain during repeated compressive loading at an increasing stress amplitude for carbon-fiber latex cement paste at 28 days of curing. Fig. 3(b) shows the corresponding variation of stress and strain during the repeated loading. The strain varies linearly with the stress up to the highest stress amplitude (Fig. 3(b)). The strain returns to zero at the end of each cycle of loading. The resistivity decreases upon loading in every cycle (due to fiber push-in) and increases upon unloading in every cycle (due to fiber pull-out). The resistivity has a net increase after the first cycle, due to damage. Little further damage occurs in subsequent cycles, as shown by the resistivity after unloading not increasing much after the first cycle. The greater the strain amplitude, the more is the resistivity decrease during loading, although the resistivity and strain are not linearly related. The effects of Fig. 3 were similarly observed in carbon-fiber silica-fume cement paste at 28 days of curing.

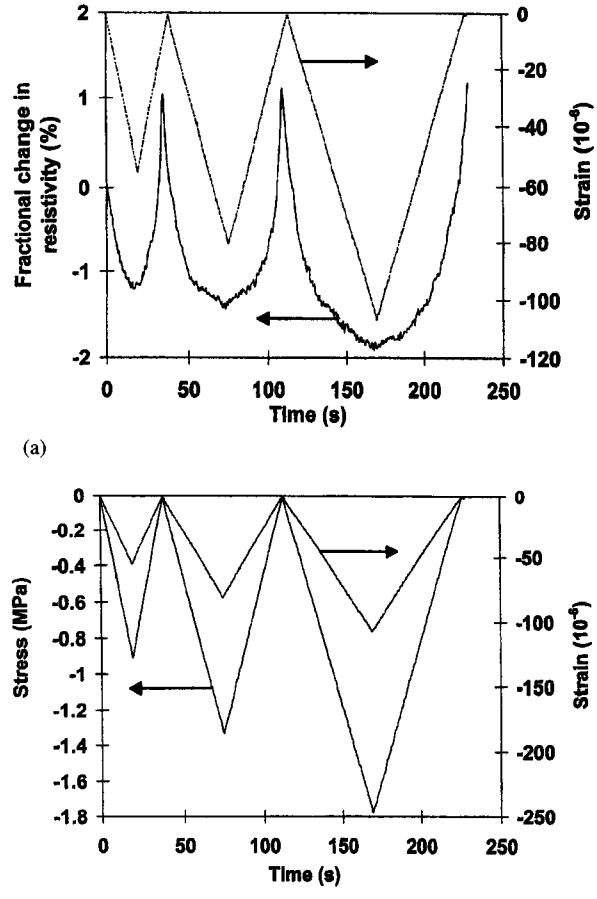

Fig. 3. Variation of the fractional change in volume electrical resistivity with time (a), of the stress with time (b), and of the strain (negative for compressive strain) with time (a,b) during dynamic compressive loading at increasing stress amplitudes within the elastic regime for carbon-fiber latex cement paste at 28 days of curing.

Figures 4 and 5 show the fractional changes in the longitudinal and transverse resistivities, respectively, for carbon-fiber silica-fume cement paste at 28 days of curing during repeated unaxial tensile loading at increasing strain amplitudes. The strain essentially returns to zero at the end of each cycle, indicating elastic deformation. The longitudinal strain is positive (i.e., elongation); the transverse strain is negative (i.e., shrinkage due to the Poisson Effect). Both longitudinal and transverse resistivities increase reversibly upon uniaxial tension. The reversibility of both strain and resistivity is more complete in the longitudinal direction than the transverse direction. The gage factor is 89 and -59 for the longitudinal and transverse resistances respectively.

Figures 6 and 7 show corresponding results for silica-fume cement paste. The strain is essentially totally reversible in both the longitudinal and transverse directions, but the resistivity is only partly reversible in both directions, in contrast to the reversibility of the resistivity when fibers are present (Figs. 4 and 5). As in the case with fibers, both longitudinal and transverse resistivities increase upon uniaxial tension. However, the gage factor is only 7.2 and -7.1 for Figs. 6 and 7 respectively.

Comparison of Figs. 4 and 5 (with fibers) with Figs. 6 and 7 (without fibers) shows that fibers greatly enhance the magnitude and reversibility of the resistivity effect. The gage factors are much smaller in magnitude when fibers are absent.

The increase in both longitudinal and transverse resistivities upon uniaxial tension for cement pastes, whether with or without fibers, is attributed to defect (e.g., microcrack) generation. In the presence of fibers, fiber bridging across microcracks occurs and slight fiber pull-out occurs upon tension, thus enhancing the possibility of microcrack closing and causing more reversibility in the resistivity change. The fibers are much more electrically conductive than the cement matrix. The presence of the fibers introduces inter-

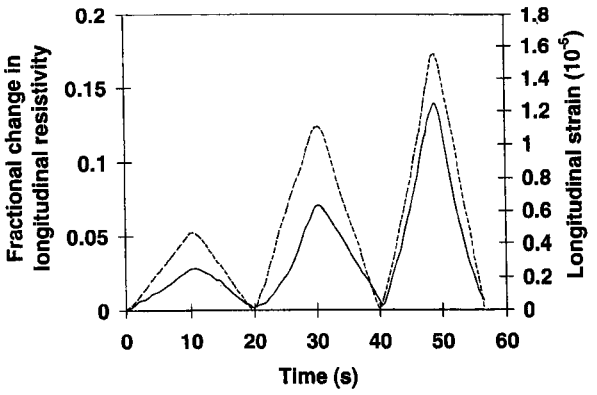

Fig. 4. Variation of the fractional change in longitudinal electrical resistivity with time (solid curve) and of the strain with time (dashed curve) during dynamic uniaxial tensile loading at increasing stress amplitudes within the elastic regime for carbon-fiber silica-fume cement paste.

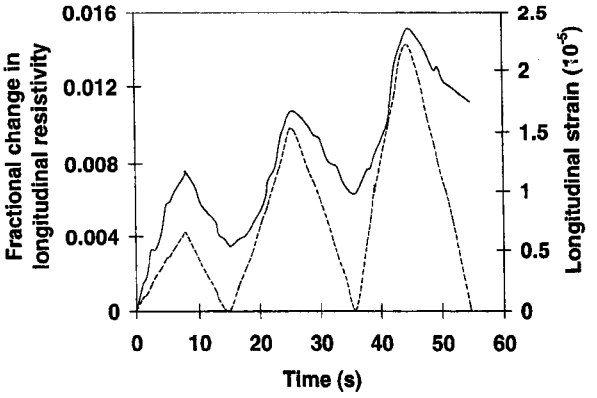

Fig. 6. Variation of the fractional change in longitudinal electrical resistivity with time (solid curve) and of the strain with time (dashed curve) during dynamic uniaxial tensile loading at increasing stress amplitudes within the elastic regime for silica-fume cement paste.

faces between fibers and matrix. The degradation of the fiber-matrix interface due to fiber pull-out or other mechanisms is an additional type of defect generation which will increase the resistivity of the composite. Therefore, the presence of fibers greatly increases the gage factor.

The transverse resistivity increases upon uniaxial tension, even though the Poisson Effect causes the transverse strain to be negative. This means that the effect of the transverse resistivity increase overshadows the effect of the transverse shrinkage. The resistivity increase is a consequence of the uniaxial tension. In contrast, under uniaxial compression, the resistance in the stress direction decreases at 28 days of curing. Hence, the effects of uniaxial tension on the transverse resistivity and of uniaxial compression on the longitudinal resistivity are different; the gage factors are negative and positive for these cases respectively.

The similarity of the resistivity change in longitudinal and transverse directions under uniaxial tension suggests similarity for other directions as well. This means that the resistance can be measured in any direction in order to sense the occurrence of tensile loading. Although the gage factor is comparable in both

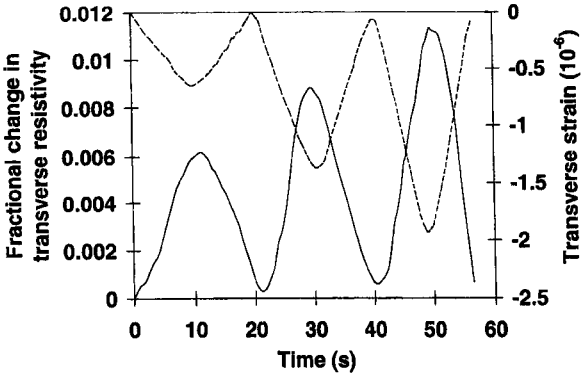

Fig. 5. Variation of the fractional change in transverse electrical resistivity with time (solid curve) and of the strain with time (dashed curve) during dynamic uniaxial tensile loading at increasing stress amplitudes within the elastic regime for carbon-fiber silica-fume cement paste.

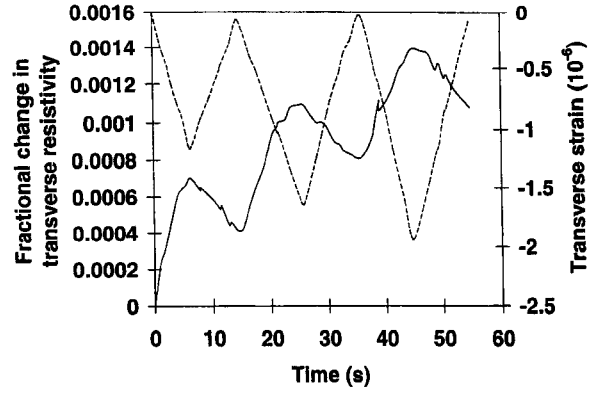

Fig. 7. Variation of the fractional change in transverse electrical resistivity with time (solid curve) and of the strain with time (dashed curve) during dynamic uniaxial tensile loading at increasing stress amplitudes within the elastic regime for silica-fume cement paste.

longitudinal and transverse directions, the fractional change in resistance under uniaxial tension is much higher in the longitudinal direction than the transverse direction. Thus, the use of the longitudinal resistance for practical self-sensing is preferred.

Damage Sensor

Concrete, whether with or without admixtures, is capable of sensing major and minor damage—even damage during elastic deformation—due to the electrical resistivity increase that accompanies damage [44,48,64–66]. That both strain and damage can be sensed simultaneously through resistance measurement means that the strain/stress condition (during dynamic loading) under which damage occurs can be obtained, thus facilitating damage origin identification. Damage is indicated by a resistance increase, which is larger and less reversible when the stress amplitude is higher. The resistance increase can be a sudden increase during loading. It can also be a gradual shift of the baseline resistance.

Fig. 8(a) [65] shows the fractional change in resistivity along the stress axis as well as the strain during repeated compressive loading at an increasing stress amplitude for plain cement paste at 28 days of curing. Fig. 8(b) shows the corresponding variation of stress and strain during the repeated loading. The strain varies linearly with the stress up to the highest stress amplitude (Fig. 8(b)). The strain returns to zero at the end of each cycle of loading. During the first loading, the resistivity increases due to damage initiation. During the subsequent unloading, the resistivity continues to increase, probably due to opening of the microcracks generated during loading. During the second loading, the resistivity decreases slightly as the stress increases up to the maximum stress of the first cycle (probably due to closing of the microcracks) and then increases as the stress increases beyond this value (probably due to the generation of additional microcracks). During unloading in the second cycle, the resistivity increases significantly (probably due to opening of the microcracks). During the third loading, the resistivity essentially does not change (or decreases very slightly) as the stress increases to the maximum stress of the third cycle (probably due to the balance between microcrack generation and microcrack closing). Subsequent unloading causes the resistivity to increase

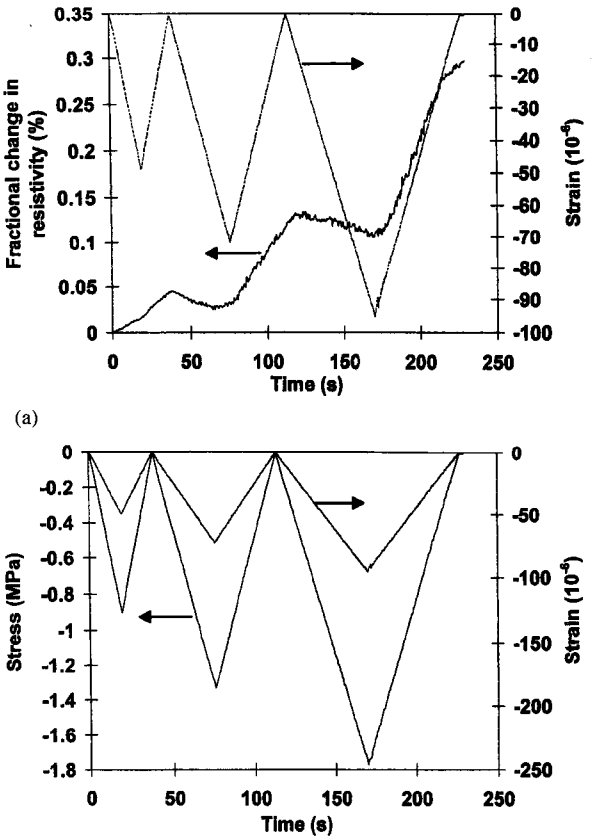

Fig. 8. Variation of the fractional change in electrical resistivity with time (a), of the stress with time (b), and of the strain (negative for compressive strain) with time (a,b) during dynamic compressive loading at increasing stress amplitudes within the elastic regime for silica-fume cement paste at 28 days of curing.

very significantly (probably due to opening of the microcracks).

Fig. 9 shows the fractional change in resistance, strain and stress during repeated compressive loading at increasing and decreasing stress amplitudes for carbon fiber (0.18 vol.%) concrete (with fine and coarse aggregates) at 28 days of curing. The highest stress amplitude is 60% of the compressive strength. A group of cycles in which the stress amplitude increases cycle by cycle and then decreases cycle by cycle back to the initial low stress amplitude is hereby referred to as a group. Fig. 9 shows the results for three groups. The strain returns to zero at the end of each cycle for any of the stress amplitudes, indicating elastic behavior. The resistance decreases upon loading in each cycle, as in Fig. 3. An extra peak at the maximum stress of a cycle grows as the stress amplitude increases, resulting in

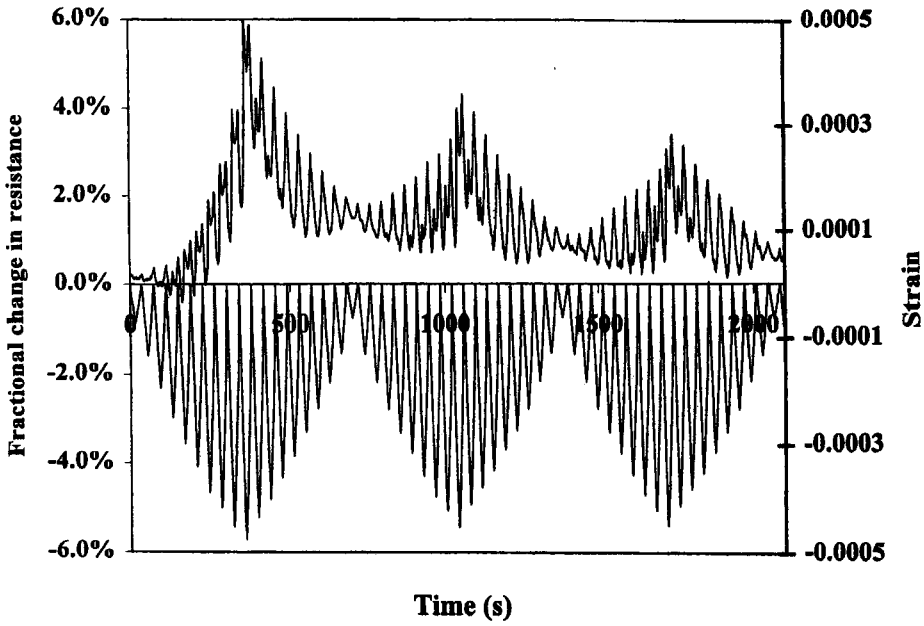

(a)

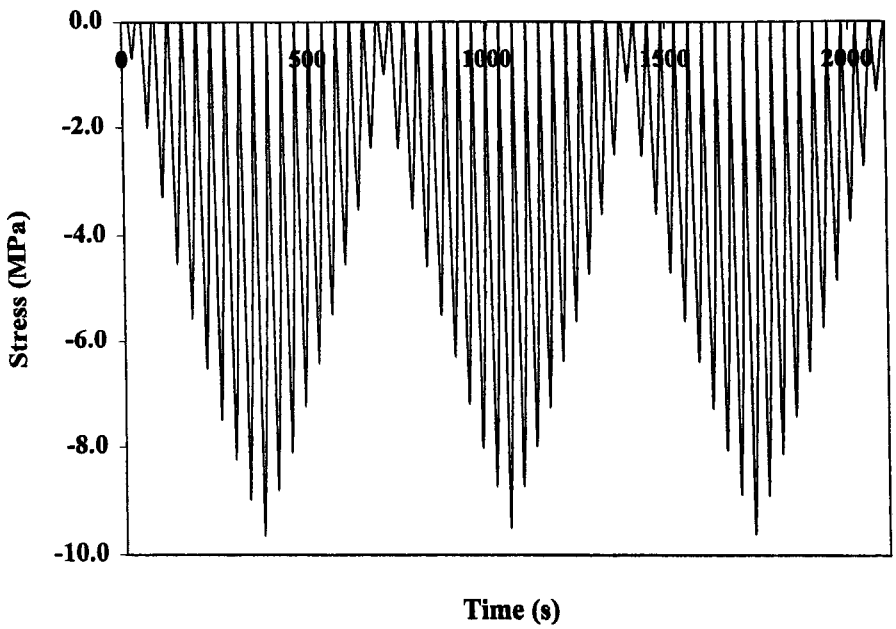

(b)

Fig. 9. Fractional change in resistance (a), strain (a) and stress (b) during repeated compressive loading at increasing and decreasing stress amplitudes, the highest of which was 60% of the compressive strength, for carbon fiber concrete at 28 days of curing.

two peaks per cycle. The original peak (strain induced) occurs at zero stress, while the extra peak (damage induced) occurs at the maximum stress. Hence, during loading from zero stress within a cycle, the resistance drops and then increases sharply, reaching the maximum resistance of the extra peak at the maximum stress of the cycle. Upon subsequent unloading, the resistance decreases and then increases as unloading continues, reaching the maximum resistance of the original peak at zero stress. In the part of this group

where the stress amplitude decreases cycle by cycle, the extra peak diminishes and disappears, leaving the original peak as the sole peak. In the part of the second group where the stress amplitude increases cycle by cycle, the original peak (peak at zero stress) is the sole peak, except that the extra peak (peak at the maximum stress) returns in a minor way (more minor than in the first group) as the stress amplitude increases. The extra peak grows as the stress amplitude increases, but, in the part of the second group in which the stress amplitude decreases cycle by cycle, it quickly diminishes and vanishes, as in the first group. Within each group, the amplitude of resistance variation increases as the stress amplitude increases and decreases as the stress amplitude subsequently decreases.

The greater the stress amplitude, the larger and the less reversible is the damage-induced resistance increase (the extra peak). If the stress amplitude has been experienced before, the damage-induced resistance increase (the extra peak) is small, as shown by comparing the result of the second group with that of the first group (Fig. 9), unless the extent of damage is large (Fig. 10 for a highest stress amplitude of >90% of the compressive strength). When the damage is extensive (as shown by a modulus decrease), damage-induced resistance increase occurs in every cycle, even at a decreasing stress amplitude, and it can overshadow the strain-induced resistance decrease (Fig. 10). Hence, the damage-induced resistance increase occurs mainly during loading (even within the elastic regime), particularly at a stress above that in prior cycles, unless the stress amplitude is high and/or damage is extensive.

At a high stress amplitude, the damage-induced resistance increase cycle by cycle as the stress amplitude increases causes the baseline resistance to increase irreversibly (Fig. 10). The baseline resistance in the regime of major damage (with a decrease in modulus) provides a measure of the extent of damage (i.e., condition monitoring). This measure works in the loaded or unloaded state. In contrast, the measure using the damage-induced resistance increase (Fig. 9) works only during stress increase and indicates the occurrence of damage (whether minor or major) as well as the extent of damage.

Thermistor

A thermistor is a thermometric device consisting of a material (typically a simiconductor, but in this case a cement paste) whose electrical resistivity decreases with rise in temperature. The carbon fiber concrete described above for strain sensing is a thermistor due to its resistivity decreasing reversibly with increasing temperature [59]; the sensitivity is comparable to that of semiconductor thermistors. (The effect of temperature will need to be compensated in using the concrete as a strain sensor.) Without fibers, the sensitivity is much lower [59,60].

Figure 11 [59] shows the current-voltage characteristic of carbon-fiber (0.5% by weight of cement) silica-fume (15% by weight of cement) cement paste at 38°C during stepped heating. The characteristic is linear below 5 V and deviates positively from linearity beyond 5 V. The resistivity is obtained from the slope of the linear portion. The voltage at which the characteristic starts to deviate from linearity is referred to as the critical voltage.

Figure 12 shows a plot of the resistivity vs. temperature during heating and cooling for carbon-fiber silica-fume cement paste. The resistivity decreases upon heating and the effect is quite reversible upon cooling. That the resistivity is slightly increased after a heating-cooling cycle is probably due to thermal degradation of the material. Fig. 13 shows the Arrhenius plot of log conductivity (conductivity = 1/resistivity) vs. reciprocal absolute temperature. The slope of the plot gives the activation energy, which is 0.390 ± 0.014 and 0.412 ± 0.017 eV during heating and cooling respectively.

Results similar to those of carbon-fiber silica-fume cement paste were obtained with carbon-fiber (0.5% by weight of cement) latex (20% by weight of cement) cement paste, silica-fume cement paste, latex cement paste and plain cement paste. However, for all these four types of cement paste, (i) the resistivity is higher by about an order of magnitude, and (ii) the activation energy is lower by about an order of magnitude, as shown in Table 1. The critical voltage is higher when fibers are absent (Table 1).

Thermoelectric Device

The Seebeck [61–63,97] effect is a thermoelectric effect which is the basis for thermocouples for temperature measurement. This effect involves charge carriers moving from a hot point to a cold point within a material, thereby resulting in a voltage difference between the two points. The Seebeck coefficient is the voltage

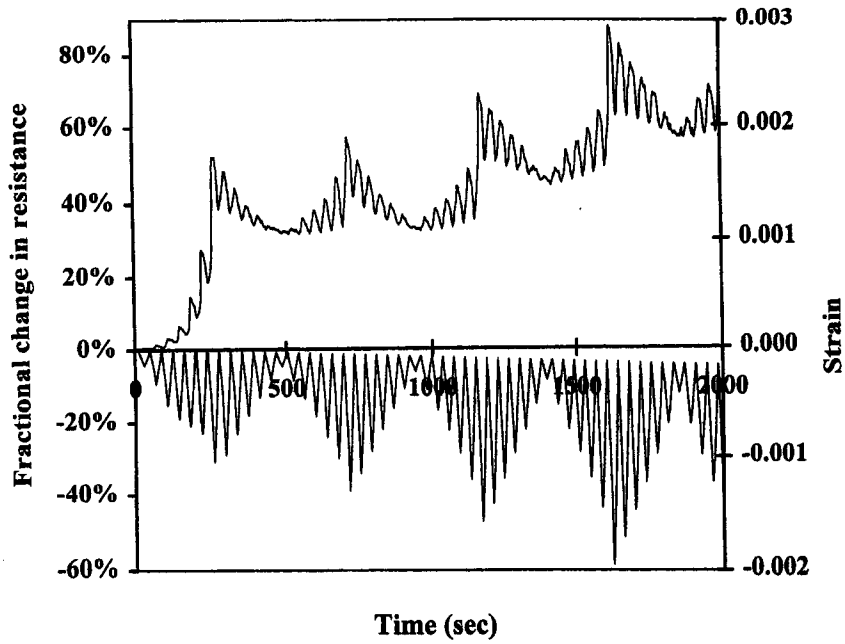

(a)

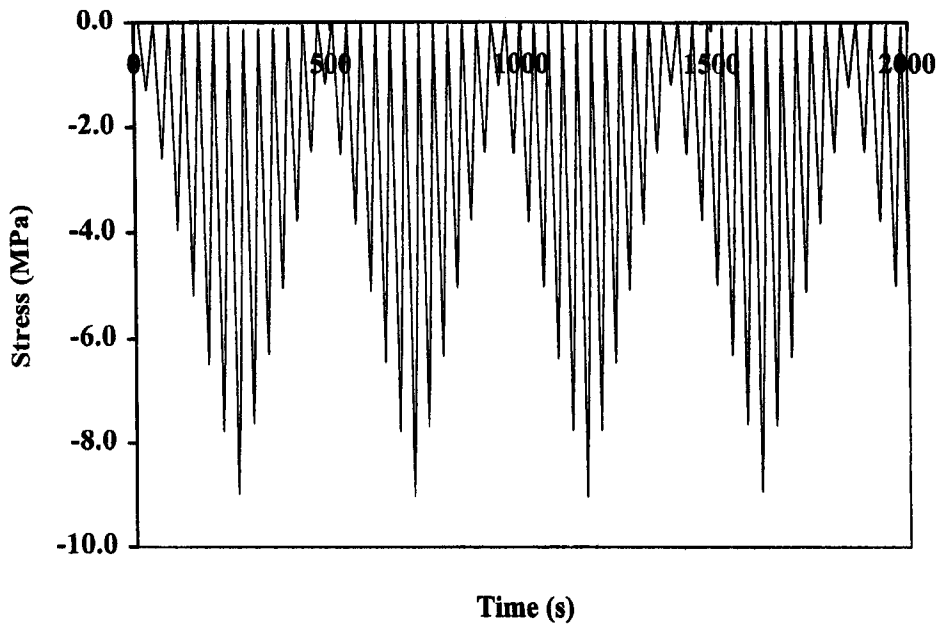

(b)

Fig. 10. Fractional change in resistance (a), strain (a) and stress (b) during repeated compressive loading at increasing and decreasing stress amplitudes, the highest of which was >90% of the compressive strength, for carbon fiber concrete at 28 days of curing.

difference per unit temperature difference between the two points. Negative carriers (electrons) make it more positive and positive carriers (holes) make it more negative.

The Seebeck effect in carbon fiber reinforced cement paste involves electrons and/or ions from the cement matrix [63] and holes from the fibers [61,62], such that the two contributions are equal at the percolation threshold, a fiber content between 0.5% and 1.0% by weight of cement [63]. The hole contribution

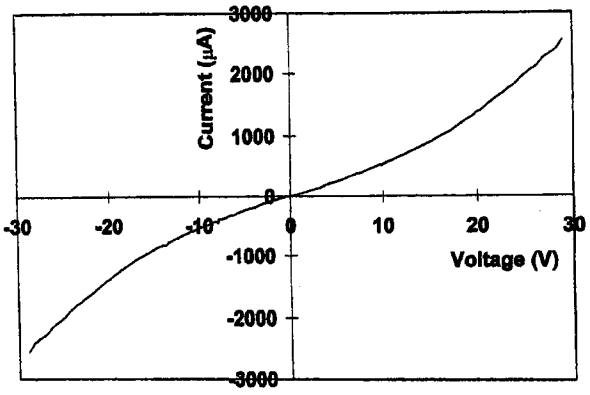

Fig. 11. Current-voltage characteristic of carbon-fiber silica-fume cement paste at 38°C during stepped heating.

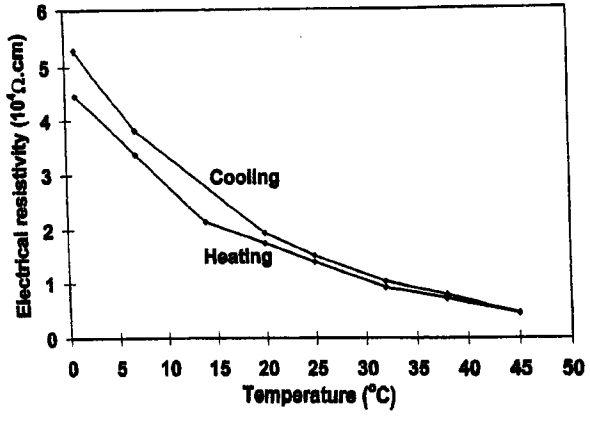

Fig. 12. Plot of volume electrical resistivity vs. temperature during heating and cooling for carbon-fiber silica-fume cement paste.

increases monotonically with increasing fiber content below and above the percolation threshold [63].

Due to the free electrons in a metal, cement containing metal fibers such as steel fibers is even more

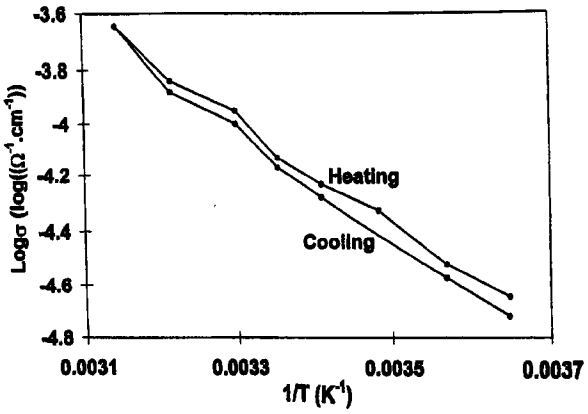

Fig. 13. Arrhenius plot of log electrical conductivity vs. reciprocal absolute temperature for carbon-fiber silica-fume cement paste.

positive in the thermoelectric power than cement without fiber [97]. The attainment of a very negative thermoelectric power is attractive, since a material with a positive thermoelectric power and a material with negative thermoelectric power are two very dissimilar materials, the junction of which is a thermocouple junction. (The greater the dissimilarity, the more sensitive is the thermocouple).

Table 2 and Fig. 14 show the thermopower results. The absolute thermoelectric power is much more positive for all the steel-fiber cement pastes compared to all the carbon-fiber cement pastes. An increase of the steel fiber content from 0.5% to 1.0% by weight of cement increases the magnitude of the absolute thermoelectric power, whether silica fume (or latex) is present or not. An increase of the steel fiber content also increases the reversibility and linearity of the change in Seebeck voltage with the temperature difference between the hot and cold ends, as shown by comparing the values of the Seebeck coefficient obtained during

Table 1. Resistivity, critical voltage and activation energy of five types of cement paste.

			Activation energy (eV)	
Formulation	Resistivity at 20°C (Ω.cm)	Critical voltage at 20°C (V)	Heating	Cooling
Plain	$(4.87 \pm 0.37) \times 10^5$	10.80 ± 0.45	0.040 ± 0.006	0.122 ± 0.006
Silica fume	$(6.12 \pm 0.15) \times 10^5$	11.60 ± 0.37	0.035 ± 0.003	0.084 ± 0.004
Carbon fibers + silica fume	$(1.73 \pm 0.08) \times 10^4$	8.15 ± 0.34	0.390 ± 0.014	0.412 ± 0.017
Latex	$(6.99 \pm 0.12) \times 10^5$	11.80 ± 0.31	0.017 ± 0.001	0.025 ± 0.002
Carbon fibers + latex	$(9.64 \pm 0.08) \times 10^4$	8.76 ± 0.35	0.018 ± 0.001	0.027 ± 0.002

Table 2. Volume electical resistivity, Seebeck coefficient (μV/°C) with copper as the reference, and the absolute thermoelectric power (μV/°C) of various cement pastes with steel fibers (S_f) or carbon fibers (C_f).

			Heating		Cooling	
Cement paste	Volume fraction fibers	Resistivity (Ω. cm)	Seebeck coefficient	Absolute thermoelectric power	Seebeck coefficient	Absolute thermoelectric power
Plain	0	$(4.7 \pm 0.4) \times 10^5$	$+0.35 \pm 0.03$	-1.99 ± 0.03	$+0.38 \pm 0.05$	-1.96 ± 0.05
SF	0	$(5.8 \pm 0.4) \times 10^5$	$+0.31 \pm 0.02$	-2.03 ± 0.02	$+0.36 \pm 0.03$	-1.98 ± 0.03
L	0	$(6.8 \pm 0.6) \times 10^5$	$+0.28 \pm 0.02$	-2.06 ± 0.02	$+0.30 \pm 0.02$	-2.04 ± 0.02
S_f (0.5*)	0.10%	$(7.8 \pm 0.5) \times 10^4$	-51.0 ± 4.8	-53.3 ± 4.8	-45.3 ± 4.4	-47.6 ± 4.4
S_f (1.0*)	0.20%	$(4.8 \pm 0.4) \times 10^4$	-56.8 ± 5.2	-59.1 ± 5.2	-53.7 ± 4.9	-56.0 ± 4.9
S_f (0.5*) + SF	0.10%	$(5.6 \pm 0.5) \times 10^4$	-54.8 ± 3.9	-57.1 ± 3.9	-52.9 ± 4.1	-55.2 ± 4.1
S_f (1.0*) + SF	0.20%	$(3.2 \pm 0.3) \times 10^4$	-66.2 ± 4.5	-68.5 ± 4.5	-65.6 ± 4.4	-67.9 ± 4.4
S_f (0.5*) + L	0.085%	$(1.4 \pm 0.1) \times 10^5$	-48.1 ± 3.2	-50.4 ± 3.2	-45.4 ± 2.9	-47.7 ± 2.9
S_f (1.0*) + L	0.17%	$(1.1 \pm 0.1) \times 10^5$	-55.4 ± 5.0	-57.7 ± 5.0	-54.2 ± 4.5	-56.5 ± 4.5
C_f (0.5*) + SF	0.48%	$(1.5 \pm 0.1) \times 10^4$	$+1.45 \pm 0.09$	-0.89 ± 0.09	$+1.45 \pm 0.09$	-0.89 ± 0.09
C_f (1.0*) + SF	0.95%	$(8.3 \pm 0.5) \times 10^2$	$+2.82 \pm 0.11$	$+0.48 \pm 0.11$	$+2.82 \pm 0.11$	$+0.48 \pm 0.11$
C_f (0.5*) + L	0.41%	$(9.7 \pm 0.6) \times 10^4$	$+1.20 \pm 0.05$	-1.14 ± 0.05	$+1.20 \pm 0.05$	-1.14 ± 0.05
C_f (1.0*) + L	0.82%	$(1.8 \pm 0.2) \times 10^3$	$+2.10 \pm 0.08$	-0.24 ± 0.08	$+2.10 \pm 0.08$	-0.24 ± 0.08

*% by weight of cement
SF: silica fume
L: latex

heating and cooling in Table 2. The values obtained during heating and cooling are close for the paste with the higher steel fiber content, but are not so close for the pastes with the lower steel fiber content. In contrast, for pastes with carbon fibers in place of steel fibers, the change in Seebeck voltage with the temperature difference is highly reversible for both carbon fiber contents of 0.5% and 1.0% by weight of cement, as shown in Table 2 by comparing the values of the Seebeck coefficient obtained during heating and cooling.

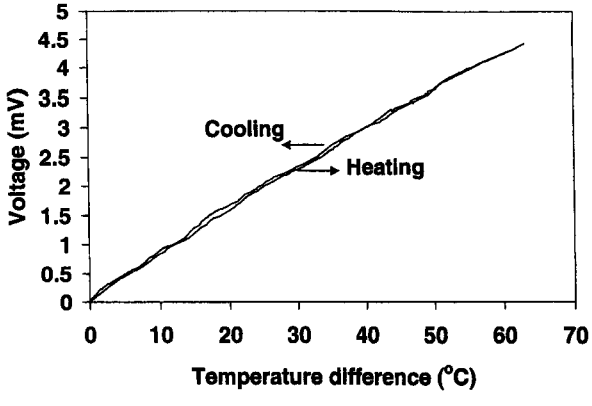

Fig. 14. Variation of the Seebeck voltage (with copper as the reference) vs. the temperature difference during heating and cooling for steel-fiber silica-fume cement paste containing steel fibers in the amount of 1.0% by weight of cement.

Table 2 shows that the volume electrical resistivity is much higher for the steel-fiber cement pastes than the corresponding carbon fiber cement pastes. This is attributed to the much lower volume fraction of fibers in the former (Table 2). An increase in the steel or carbon fiber content from 0.5% to 1.0% by weight of cement decreases the resistivity, though the decrease is more significant for the carbon fiber case than the steel fiber case. That the resistivity decrease is not large when the steel fiber content is increased from 0.5% to 1.0% by weight of cement and that the resistivity is still high at a steel fiber content of 1.0% by weight of cement suggest that a steel fiber content of 1.0% by weight of cement is below the percolation threshold.

Whether with or without silica fume (or latex), the change of the Seebeck voltage with temperature is more reversible and linear at a steel fiber content of 1.0% by weight of cement than at a steel fiber content of 0.5% by weight of cement. This is attributed to the larger role of the cement matrix at the lower steel fiber content and the contribution of the cement matrix to the irreversibility and non-linearity. Irreversibility and

non-linearity are particularly significant when the cement paste contains no fiber.

From the practical point of view, the steel-fiber silica-fume cement paste containing steel fibers in the amount of 1.0% by weight of cement is particularly attractive for use in temperature sensing, as the magnitude of the absolute thermoelectric power is the highest (-68 μV/°C) and the variation of the Seebeck voltage with the temperature difference between the hot and cold ends is reversible and linear. The absolute thermoelectric power is as high as those of commercial thermocouple materials.

Conclusion

Cement-based electronics provide electrical circuit elements, including conductor and diode (pn-junction), in addition to strain and damage sensors, thermistor and thermoelectric device. This emerging technology provides the basis for the use of concrete structures for electronic functions.

Acknowledgement

This work was supported in part by the National Science Foundation, U.S.A.

References

1. J. W. Newman, Int. SAMPE Symp. Exhib., SAMPE, Covina, CA, **32,** 938 (1987).
2. S. Furukawa, Y. Tsuji, and S. Otani, *Proc. 30th Japan Congress on Materials Research,* Soc. of Materials Science, Kyoto, Jpn. (1987) p. 149.
3. K. Saito, N. Kawamura, and Y. Kogo, *Advanced Materials: The Big Payoff,* National SAMPE Technical Conf., Covina, CA, **21,** 796 (1989).
4. S. Wen and D.D.L. Chung, *Cen. Concr. Res.,* **29** 445 (1999).
5. T. Sugama, L. E. Kukacka, N. Carciello, and D. Stathopoulos, *Cem. Concr. Res.,* **19** 355 (1989).
6. X. Fu, W. Lu, and D.D.L. Chung, *Cem. Concr. Res.,* **26** 1007 (1996).
7. X. Fu, W. Lu, and D.D.L. Chung, *Carbon,* **36,** 1337 (1998).
8. Y. Xu and D.D.L. Chung, *Cem. Concr. Res.,* **29,** 773 (1999).
9. T. Yamada, K. Yamada, R. Hayashi, and T. Herai, *Int. SAMPE Symp. Exhib.,* Covina, CA, **36,** 362 (1991).
10. T. Sugama, L. E. Kukacka, N. Carciello, and B. Galen, *Cem. Concr. Res.,* **18,** 290 (1988).
11. B. K. Larson, L. T. Drzal, and P. Sorousian, *Composites,* **21,** 205 (1990).
12. A. Katz, V.C. Li, and A. Kazmer, *J. Materials Civil Eng.,* **7,** 125 (1995).
13. S. B. Park and B. I. Lee, *Cem. Concr. Composites* **15,** 153 (1993).
14. P. Chen, X. Fu, and D.D.L. Chung, *ACI Mater. J.,* **94,** 147 (1997).
15. P. Chen and D.D.L. Chung, *Composites,* **24,** 33 (1993).
16. A. M. Brandt and L. Kucharska, *Materials for the New Millennium,* Proc. Mater. Eng. Conf., ASCE, New York, NY, **1,** 271. (1996).
17. H. A. Toutanji, T. El-Korchi, R. N. Katz, and G. L. Leatherman, *Cem. Concr. Res.,* **23,** 618 (1993).
18. N. Banthia and J. Sheng, *Cem. Concr. Composites,* **18,** 251 (1996).
19. H. A. Toutanji, T. El-Korchi, and R. N. Katz, *Com. Con. Composites,* **16,** 15 (1994).
20. S. Akihama, T. Suenaga, and T. Banno, *Int. J. Cem. Composites & Lightweight Concrete,* **6,** 159 (1984).
21. M. Kamakura, K. Shirakawa, K. Nakagawa, K. Ohta, and S. Kashihara, *Sumitomo Metals* (1983).
22. A. Katz and A. Bentur, *Cem. Concr. Res.,* **24,** 214 (1994).
23. Y. Ohama and M. Amano, Proc. 27th Japan Congress on Materials Research, Soc. Mater. Sci., Kyoto, Japan, p. 187 (1983).
24. Y. Ohama, M. Amano, and M. Endo, *Concrete Int.: Design & Construction,* **7,** 58 (1985).
25. K. Zayat and Z. Bayasi, *ACI Mater. J.,* **93,** 178 (1996).
26. P. Soroushian, F. Aouadi, and M. Nagi, *ACI Mater. J.,* **88,** 11 (1991).
27. B. Mobasher and C. Y. Li, *ACI Mater. J.,* **93,** 284 (1996).
28. N. Banthia, A. Moncef, K. Chokri, and J. Sheng, *Can. J. Civil Eng.,* **21,** 999 (1994).
29. B. Mobasher and C. Y. Li, *Infrastructure: New Materials and Methods of Repair,* Proc. Mater. Eng. Conf., n 804, ASCE, New York, NY, p. 551 (1994).
30. P. Soroushian, M. Nagi, and J. Hsu, *ACI Mater. J.,* **89,** 267 (1992).
31. P. Soroushian, *Construction Specifier,* **43,** 102 (1990).
32. A. K. Lal, *Batiment Int./Building Research & Practice,* **18,** 153 (1990).
33. S. B. Park, B. I. Lee, and Y. S. Lim, *Cem. Concr. Res.,* **21,** 589 (1991).
34. S. B. Park and B. I. Lee, *High Temperatures—High Pressures,* **22,** 663 (1990).
35. P. Soroushian, Mohamad Nagi, and A. Okwuegbu, *ACI Mater. J.,* **89,** 491 (1992).
36. M. Pigeon, M. Azzabi, and R. Pleau, *Cem. Concr. Res.,* **26,** 1163 (1996).
37. N. Banthia, K. Chokri, Y. Ohama, and S. Mindess, *Adv. Cem. Based Mater.,* **1,** 131 (1994).
38. N. Banthia, C. Yan, and K. Sakai, *Com. Concr. Composites,* **20,** 393 (1998).
39. T. Urano, K. Murakami, Y. Mitsui, and H. Sakai, *Composites—Part A: Applied Science & Manufacturing,* **27,** 183 (1996).
40. A. Ali and R. Ambalavanan, *Indian Concrete J.,* **72,** 669 (??).
41. P. Chen, X. Fu, and D.D.L. Chung, *Cem. Concr. Res.,* **25,** 491 (1995).
42. M. Zhu and D.D.L. Chung, *Cem. Concr. Res.,* **27,** 1829 (1997).
43. M. Zhu, R. C. Wetherhold, and D.D.L. Chung, *Cem. Concr. Res.,* **27,** 437 (1997).

44. P. Chen and D.D.L. Chung, *Smart Mater. Struct.*, **2,** 22 (1993).
45. P. Chen and D.D.L. Chung, *Composites,* Part B, **27B,** 11 (1996).
46. P. Chen and D.D.L. Chung, *J. Am. Ceram. Soc.*, **78,** 816 (1995).
47. D.D.L. Chung, *Smart Mater. Struct.*, **4,** 59 (1995).
48. P. Chen and D.D.L. Chung, *ACI Mater. J.*, **93,** 341 (1996).
49. X. Fu and D.D.L. Chung, *Cem. Concr. Res.*, **26,** 15 (1996).
50. X. Fu, E. Ma, D.D.L. Chung and W. A. Anderson, *Cem. Concr. Res.*, **27,** 845 (1997).
51. X. Fu and D.D.L. Chung, *Cem. Concr. Res.*, **27,** 1313 (1997).
52. X. Fu, W. Lu and D.D.L. Chung, *Cem. Concr. Res.*, **28,** 183 (1998).
53. D.D.L. Chung, *TANSO* **190,** 300 (1999).
54. Z. Shi and D.D.L. Chung, *Cem. Concr. Res.*, **29,** 435 (1999).
55. Q. Mao, B. Zhao, D. Sheng, and Z. Li, *J. Wuhan U. Tech. (Mater. Sci. Ed.),* **11,** 41 (1996).
56. Q. Mao, B. Zhao, D. Shen, and Z. Li, *Fuhe Cailiao Xuebao/Acta Materiae Compositae Sinica,* **13,** 8 (1996).
57. M. Sun, Q. Mao, and Z. Li, *J. Wuhan U. Tech. (Mater. Sci. Ed.),* **13,** 58 (1998).
58. B. Zhao, Z. Li, and D. Wu, *J. Wuhan Univ. Tech. (Mater. Sci. Ed.),* **10,** 52 (1995).
59. S. Wen and D.D.L. Chung, *Cem. Concr. Res.*, **29,** 961 (1999).
60. W.J. McCarter, *J. Am. Ceram. Soc.*, **78,** 411 (1995).
61. M. Sun, Z. Li, Q. Mao and D. Shen, *Cem. Concr. Res.*, **28,** 549 (1998).
62. M. Sun, Z. Li, Q. Mao, and D. Shen, *Cem. Concr. Res.*, **28,** 1707 (1998).
63. S. Wen and D.D.L. Chung, *Cem. Concr. Res.*, **29,** 1989 (1999).
64. D. Bontea, D.D.L. Chung, and G.C. Lee, *Cem. Concr. Res.*, **30,** 651 (2000).
65. S. Wen and D.D.L. Chung, *Cem. Concr. Res.*, in press.
66. J. Lee and G. Batson, *Materials for the New Millenium,* Proc. 4th Mater. Eng. Conf., ASCE, New York, NY, **2,** 887 (1996).
67. X. Fu and D.D.L. Chung, *ACI Mater. J.*, **96,** 455 (1999).
68. Y. Xu and D.D.L. Chung, *Cem. Concr. Res.*, **29,** 1117 (1999).
69. Y. Shinozaki, *Adv. Mater.: Looking Ahead to the 21st* Century, Proc. 22nd National SAMPE Tech. Conf., SAMPE, Covina, CA, **22,** 986 (1990).
70. X. Fu and D.D.L. Chung, *Cem. Concr. Res.*, 25, 689 (1995).
71. J. Hou and D.D.L. Chung, *Cem. Concr. Res.*, **27,** 649 (1997).
72. G. G. Clemena, *Materials Performance,* **27,** 19 (1988).
73. R. J. Brousseau and G. B. Pye, *ACI Mater. J.*, **94,** 306 (1997).
74. P. Chen and D.D.L. Chung, *Smart Mater. Struct,* **2,** 181 (1993).
75. P. Chen and D.D.L. Chung, *J. Electron. Mater.*, **24,** 47 (1995).
76. X. Wang, Y. Wang and Z. Jin, *Fuhe Cailiao Xuebao/Acta Materiae Compositae Sinica,* **15,** 75 (1998).
77. N. Banthia, S. Djeridane, and M. Pigeon, *Cem. Concr. Res.*, **22,** 804 (1992).
78. P. Xie, P. Gu, and J. J. Beaudoin, *J. Mater. Sci.*, **31,** 4093 (1996).
79. Z. Shui, J. Li, F. Huang, and D. Yang, *J. Wuhan Univ. Tech. (Mater. Sci. Ed.),* **10,** 37 (1995).
80. X. Fu and D.D.L. Chung, *Cem. Concr. Res.*, **28,** 795 (1998).
81. X. Fu and D.D.L. Chung, *Carbon,* **36,** 459 (1998).
82. X. Fu and D.D.L. Chung, *Cem. Concr. Res.*, **26,** 1467 (1996); **27,** 314 (1997).
83. T. Fujiwara and H. Ujie, *Tohoku Kogyo Daigaku Kiyo, 1: Rikogakuhen,* **7,** 179 (1987).
84. Y. Shimizu, A. Nishikata, N. Maruyama, and A. Sugiyama, *Terebijon Gakkaishi/J. Inst. Television Engineers of Japan,* **40,** 780 (1986).
85. P. Chen and D.D.L. Chung, *ACI Mater. J.*, **93,** 129 (1996).
86. T. Uomoto and F. Katsuki, *Doboku Gakkai Rombun-Hokokushu/Proc. Japan Soc. Civil Engineers,* **490,** 167 (1994–1995).
87. C. M. Huang, D. Zhu, C. X. Dong, W. M. Kriven, R. Loh, and J. Huang, *Ceramic Eng. Sci. Proc.*, **17,** 258 (1996).
88. C. M. Huang, D. Zhu, X. Cong, W. M. Kriven, R. R. Loh, and J. Huang, *J. Am. Ceramic Soc.*, **80,** 2326 (1997).
89. T-J. Kim and C-K. Park, *Cem. Concr. Res.*, **28,** 955 (1998).
90. S. Igarashi and M. Kawamura, *Doboku Gakkai Rombun-Hokokushu/Proc. Japan Soc. Civil Eng.*, **502,** 83 (1994).
91. M. Z. Bayasi and J. Zeng, *ACI Structural J.*, 94, 442 (1997).
92. G. Campione, S. Mindess, and G. Zingone, *ACI Mater. J.*, **96,** 27 (1999).
93. T. Yamada, K. Yamada, and K. Kubomura, *J. Composite Mater.*, **29,** 179 (1995).
94. S. Delvasto, A. E. Naaman, and J. L. Throne, *Int. J. Cement Composites & Lightweight Concrete,* **8,** 181 (1986).
95. C. Park, Nippon Seramikkusu Kyokai *Gakujutsu Ronbunshi/J. Ceramic Soc. Japan,* **106,** 268 (1998).
96. Y. Shao, S. Marikunte, and S. P. Shah, *Concrete Int.*, **17,** 48 (1995).
97. S. Wen and D.D.L. Chung, *Cem. Concr. Res.*,**30,** 661 (2000).
98. S. Wen and D.D.L. Chung, *Cem. Concr. Res.*, in press.